Accepted Manuscript

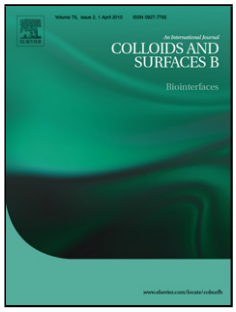

Title: Preparation and in vitro characterization of chitosan nanobubbles as theranostic agents

Author: R. Cavalli M. Argenziano E. Vigna P. Giustetto E. Torres S. Aime E. Terreno

PII: S0927-7765(15)00157-5
DOI: http://dx.doi.org/doi:10.1016/j.colsurfb.2015.03.023
Reference: COLSUB 6963

To appear in: *Colloids and Surfaces B: Biointerfaces*

Received date: 16-9-2014
Revised date: 21-1-2015
Accepted date: 8-3-2015

Please cite this article as: R. Cavalli, M. Argenziano, E. Vigna, P. Giustetto, E. Torres, S. Aime, E. Terreno, Preparation and in vitro characterization of chitosan nanobubbles as theranostic agents, *Colloids and Surfaces B: Biointerfaces* (2015), http://dx.doi.org/10.1016/j.colsurfb.2015.03.023

Graphical abstract

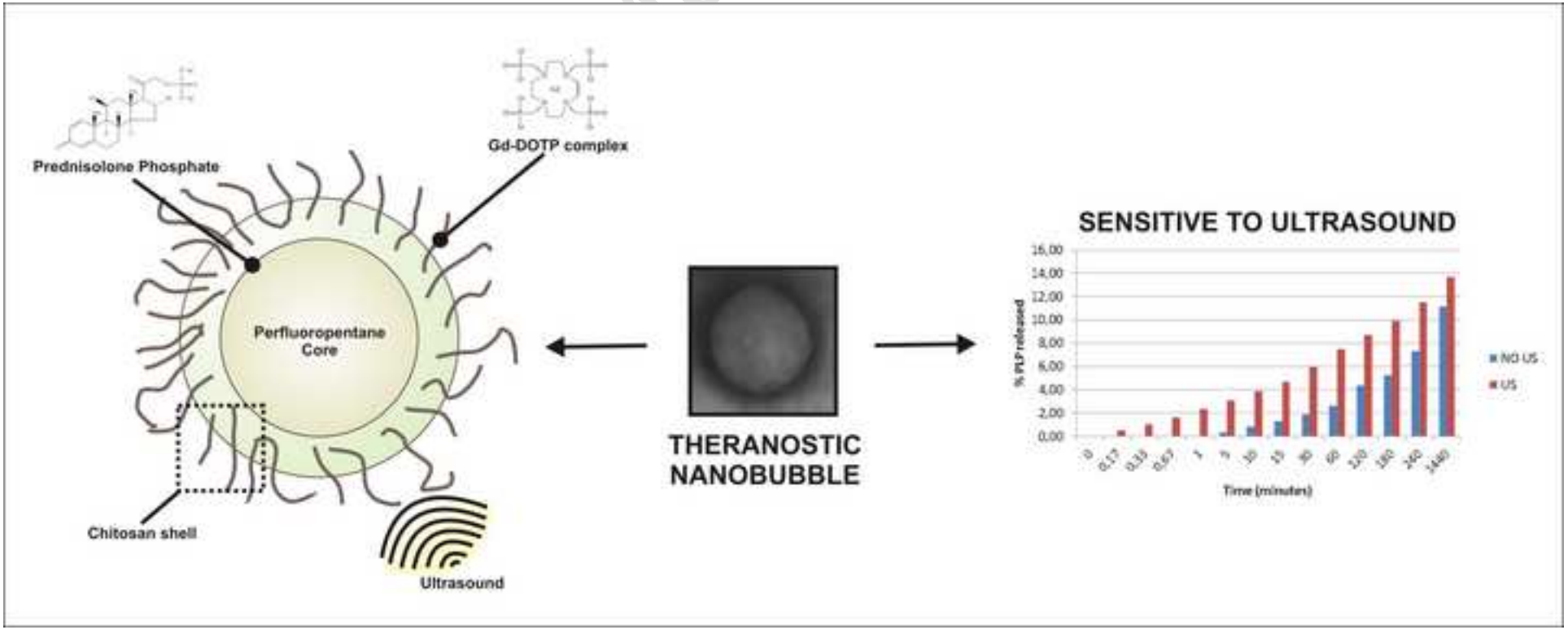

Highlights

- Theranostic chitosan-shelled and perfluoropentane-filled nanobubble system
- Efficient co-incorporation of PLP and a Gd complex, as therapeutic and MRI agent
- Prolonged *in vitro* drug release kinetics enhanced by US application
- Good *in vitro* echogenicity of the theranostic nanobubbles due to ADV phenomenon
- Ability of theranostic nanobubbles to generate positive MRI contrast

Preparation and in vitro characterization of chitosan nanobubbles as theranostic agents

R. Cavalli[1*], M. Argenziano[1], E. Vigna[1], P. Giustetto[2], E. Torres[2], S. Aime[2], E. Terreno[2*]

[1] *Dipartimento di Scienza e Tecnologia del Farmaco, Università degli Studi di Torino, via P. Giuria 9, 10125 Torino, Italy*

[2] *Dipartimento di Biotecnologie Molecolari e Scienze della Salute, Centro di Imaging Molecolare e Preclinico, Università degli Studi di Torino, via Nizza 52, 10126 Torino, Italy*

* Corresponding authors:
Roberta Cavalli
Dipartimento di Scienza e Tecnologia del Farmaco, Università degli Studi di Torino, via P. Giuria 9, 10125 Torino, Italy
Phone: +39-011-6707825
Fax: +39-011-6707687
e-mail roberta.cavalli@unito.it
Enzo Terreno
Dipartimento di Biotecnologie Molecolari e Scienze della Salute, Centro di Imaging Molecolare e Preclinico, Università degli Studi di Torino, via Nizza 52, 10126 Torino, Italy
Phone: +39-011-6706452
Fax: +39-011-6706487
e-mail: enzo.terreno@unito.it

ABSTRACT

Theranostic delivery systems are nanostructures that combine the modality of therapy and diagnostic imaging. Polymeric micro- and nanobubbles, spherical vesicles containing a gas core, have been proposed as new theranostic carriers for MRI-guided therapy. In this study, chitosan nanobubbles were purposely tuned for the co-delivery of prednisolone phosphate and a Gd (III) complex, as therapeutic and MRI diagnostic agent, respectively. Perfluoropentane was used for filling up the internal core of the formulation. These theranostic nanobubbles showed diameters of about 500 nm and a positive surface charge that allows the interaction with the negatively charged Gd-DOTP complex. Pluronic F68 was added to the nanobubble aqueous suspension as stabilizer agent. The encapsulation efficiency was good for both the active compounds, and a prolonged drug release profile was observed *in vitro*. The effect of ultrasound stimulation on prednisolone phosphate release was evaluated at 37 °C. A marked increase on drug release kinetics with no burst effect was obtained after the exposure of the system to ultrasound. Furthermore, the relaxivity of the MRI probe changed upon incorporation in the nanobubble shell, thereby offering interesting opportunity in dual MRI-US experiments. The ultrasound characterization showed a good *in vitro* echogenicity of the theranostic nanobubbles.

In summary, chitosan drug-loaded nanobubbles with Gd (III) complex bound to their shell might be considered a new platform for imaging and drug delivery with the potential of improving anti-cancer treatments.

Keywords: Gd complex, nanobubbles, MRI**,** theranosis, ultrasound, controlled release.

Introduction

A typical theranostic agent is a system that provides imaging support to a therapeutic treatment [1, 2, 3, 4].

The theranostic approach appears to be particularly relevant for improving the cure of cancer or other important diseases at an early stage, as it has the potential to image the pathological tissues and, at the same time, to monitor the delivery kinetics and biodistribution of a drug, thereby obtaining important benefits in terms of tuning therapy and doses, and reducing adverse side effects.

Nano-sized systems are promising theranostics because their sizes favor a prolonged circulation time after intravenous administration, and good loading capacity. Various nanotechnological systems have been considered for carrying imaging probes and drugs, *e.g.* polymeric nanoparticles, micelles, vesicles, and liposomes [5, 6]. Ideally, for theranostic purposes, the nanocarrier should be stable (*i.e.* no drug release in body districts different from the biological target), easily tunable, with a high payload capacity, and with multifunctional properties. Microbubbles and nanobubbles are spherical particles with a core-shell structure filled up with a gas, which gives them acoustically active properties [7, 8, 9]. Microbubbles mean diameters are generally between 1 and 8 micrometers. The shell can be mainly composed of proteins, lipids or polymers, whereas the core can be filled up with various gases. Currently, microbubbles are on the market as contrast agents for Ultrasound (US) imaging. Under US acoustic pressure, they are able to produce volumetric oscillations detectable by clinical US scanners. Besides the well established diagnostic applications [10, 11, 12], microbubbles have been recently investigated as delivery systems for drugs and genes.

Nanobubbles (NBs) are bubbles of sub-micron size, which are primarily designed to increase the stability and improve the biodistribution of the transported drug to the pathological region. Indeed, microbubbles are not able to extravasate from the bloodstream due to their larger size. Nanobubbles do and have been already investigated as gene delivery systems [13, 14, 15].

Lipid nanobubbles for US imaging detection have been proposed for the *in vivo* contrast-enhanced imaging of tumor tissues for applications in the field of drug delivery [16].

The use of MRI detectable microbubbles for theranostic purposes has been already proposed. Gd-DTPA loaded microbubbles of PLGA were designed as multimodal contrast agents for both US and MRI [17]. Albumin-based microbubbles filled with decafluorobutane gas and containing Gd-DTPA covalently linked to Human Serum Allbumin (HSA) were used to enhance the detection of inflamed sites within the vascular wall [18].

Bubbles for MRI detection has been also proposed by Feshitan *et al.*, who prepared lipid-based theranostic microbubbles loaded with a paramagnetic Gd(III) complex to guide focused ultrasound surgery [19].

Bubbles made of chitosan have been already prepared as oxygen delivery system for the potential treatment of hypoxic tissues [20, 21] and, recently, chitosan-based nanobubbles have been reported for US-triggered DNA delivery [22]. We deemed of interest to design chitosan nanobubbles as dual MRI/US theranostic tool to deliver both a MRI probe and a drug.

For this purpose, in this work a chitosan-based formulation containing prednisolone phosphate (PLP) as model drug and the paramagnetic complex Gd-DOTP as T_1-MRI agent (positive contrast) has been prepared and tested *in vitro*.

Perfluorocarbons have been used for contrast agent preparation because of their stability, biological inertness and low water solubility [23]. *In vivo*, they are excreted from lung capillaries, where they can escape from the bubble core and enter the alveolus to be exhaled. Perfluorocarbons can act as bubble stabilizer being able to increase the lifetime of bubbles in the bloodstream [24, 25].

Perfluoropentane vapor, due to the extremely low solubility in water ($4 \cdot 10^{-3}$ mol/m^3), can remain inside the bubbles and it is able to dissolve the water-soluble gases present in the blood.

For these reasons, the latter molecule was selected for the herein presented system. Furthermore, perfluoropentane can tolerate intrabubble gas pressure larger than 1 atm, thus stabilizing the system. Besides these favorable features, we selected perfluoropentane because it is liquid at room temperature (b.p.= 29 °C), thus allowing an easy preparation set up. It could convert to a gas at body temperature (37 °C), though the presence of the Laplace pressure can increase the gas boiling temperature within the nanobubble structure.

The Laplace pressure is the pressure difference between the inside and the outside of a bubble (or a droplet), given as:

$$\Delta P = P_{inside} - P_{outside} = \frac{2\sigma}{r}$$

where P_{inside} and $P_{outside}$ are the pressures inside and outside a bubble respectively, σ is the interfacial tension, and r is the bubble radius.

However, it has been demonstrated that the liquid to gas phase transition of perfluoropentane inside the nanobubbles can be activated by US through the Acoustic Droplet Vaporization (ADV) mechanism [26].

PLP is a glucocorticoid drug used for the treatment of inflammatory diseases and, in chemotherapy, to reduce adverse side effects of anticancer drugs. It was also proposed as anticancer drugs itself due to the ability to inhibit angiogenesis [27]. Recently, PLP encapsulated in liposomes showed an increased anti-tumor efficacy, which is attributed to an enhanced tumor

accumulation of the drug loaded in the liposomal formulation caused by the EPR effect [28]. More recently, an amphiphilic Gadolinium complex was added to liposomes containing PLP to obtain paramagnetic liposomes suitable for their MRI-guided visualization in mice [29]. The choice of PLP was primarily driven by its amphiphilic nature (that allows both the interaction with the bubble interface) and the presence of a negative charge (that favor the interaction with the cationic chitosan). The anionic paramagnetic complex Gd-DOTP was chosen as MRI agent, in virtue of the well-documented ability of lanthanide-complexes of DOTP ligand to interact with cationic systems [30, 31].

The aim of this work is the development of new stable theranostic chitosan-based nanobubbles containing the MR imaging (Gd-DOTP) and the drug (PLP) companions. The theranostic system is characterized *in vitro* to assess the MRI and echogenic potential.

Materials

Ethanol 96° was purchased from Carlo Erba (Milan, I). Epikuron 200® (dipalmitoyl phosphatidylcholine 95%) was a kind gift from Degussa (Hamburg, D). Palmitic acid, perfluoropentane, Pluronic F68, chitosan (Low Molecular Weight, 50-70 KDa, DD= 75-85 %), prednisolone phosphate (PLP) were purchased from Sigma Aldrich (St. Louis, MO, Usa). Gd-DOTP was kindly provided by Bracco Imaging SpA (Colleretto Giacosa (TO), Italy). Ultra-pure water was obtained using a system 1-800 Milli-Q (Millipore, F, Usa). Tetradecylphosphoric acid (C14) was synthesized as previously reported [22]. All the other reagents were of analytical grade.

Preparation of the theranostic chitosan nanobubbles

A multistep method was purposely developed to prepare the theranostic nanobubbles. Firstly, 300 microliters of an ethanolic solution of Epikuron® 200 (1 % w/w) containing a co-surfactant were added under stirring to 500 microliters of perfluoropentane at room temperature. Then, 4.8 ml of ultrapure water were slowly added to the mixture (under mild stirring) until the formation of an emulsion. Subsequently, the system was homogenized for three minutes at 12000 rpm using a high-shear homogenizer (Ultraturrax, IKA, Germany) in an ice-bath. The third step consisted of the drop-wise addition of an aqueous solution of chitosan (pH=5.0, 2.7 w/w) that formed the nanobubble polymeric shell. For tuning the formulation sizes, two different co-surfactants were tested: palmitic acid (C16) and tetradecylphosphoric acid (C14), thus obtaining two types of nanobubble formulations: C14-NB and C16-NB.

Finally, 200 μl of an aqueous solution of Gd-DOTP (Fig.1A) at the concentration of 4.4 mM were drop-wise added under stirring to the two types of pre-formed nanobubbles in aqueous suspension. The so-obtained formulations (Gd-C14-NB and Gd-C16-NB) were incubated for 30

minutes under stirring to facilitate the binding of the negatively charged Gd complex with the cationic nanobubble chitosan shell. Then, free Gd-DOTP (as well as other soluble components unbound to NBs) was removed by dia-ultrafiltration using a TCF2 system (Amicon) with a dialysis membrane cut off of 100 kDa.

After the purification, an aqueous solution of the stabilizer agent Pluronic F68 (0.01 % w/w) was added under stirring to the aqueous nanobubble suspensions.

The drug prednisolone phosphate (Fig.1A) was loaded to the NB formulation upon addition of the drug (2 mg/ml) to the ethanolic solution of Epikuron®. Then, the preparation procedure was carried out as reported above. Blank nanobubbles (C14-NB and C16-NB) were prepared as control. All the nanobubble samples were stored at 4 °C.

Determination of perfluoropentane surface tension

The surface tension of perfluropentane as such and perfluoropentane plus Epikuron 200® and PLP ethanol mixture at the same concentration used in the nanobubble preparation were measured using a K10 tensiomter (Kruss) at 25 °C.

Determination of DOTP loading capacity of nanobubbles

Preliminary experiments were carried out to determine the DOTP loading capacity of the pre-formed nanobubbles and to identify the suitable concentration for producing a detectable MRI signal. A series of nanobubbles formulated with an increasing amount of chitosan were prepared and incubated with a fixed concentration of Gd-DOTP (0.15 mM). The amount of Gd-DOTP bound to the nanobubbles was assessed by relaxometric measurements as described below. The formulation with the highest payload of Gd-DOTP was used for the subsequent experiments.

Quantitative determination of chitosan

The quantitative determination of chitosan in solution was carried out using a modified version of the fluorimetric assay method reported in the literature [32]. A calibration curve was obtained as follows: 500 microliters of a fluorescamine solution prepared in DMSO (2 mg/ml) were added to 500 microliters of a series of chitosan solutions (pH 5.0) at different concentration in the range 1-6 μg/ml. After 30 minutes of incubation in the dark, the samples were diluted using a 0.02 M KH_2PO_4 solution at pH=8.5. Then, fluorescence was measured (λ_{ex} =384 nm and λ_{em}=489 nm, Shimadzu RF 550). To determine the amount of chitosan present in the nanobubble formulation (or in the washing waters), 100 microliters of the unknown sample were diluted with 100 microliters of the fluorescamine solution. The resulting solution was treated as described above and the chitosan concentration was obtained from the calibration curve.

Quantitative determination of PLP

PLP quantification was carried out spectrophotometrically (DU 730 instrument, Beckman), measuring the absorbance at 252 nm after suitable dilution of the samples.

The PLP concentration in the samples was calculated from a calibration curve.

To obtain a calibration curve, a weighted amount of PLP was dissolved in filtered water in a volumetric flask. This stock solution was then diluted with water, to obtain a series of PLP solutions that were analyzed spectrophotometrically. A linear calibration curve was obtained over the concentration range of 0.5 - 20 μg/ml with a regression coefficient of 0.998.

Relaxometric measurements

Longitudinal water proton relaxation rates (R_{1obs}) were measured at 0.5 Tesla and 25°C on a Stelar Spinmaster spectrometer (Stelar, PV, Italy) by means of a standard inversion recovery pulse sequence. The temperature was controlled by a copper-constantan thermocouple (Stelar VTC-91).

The relaxivity (r_1) of the paramagnetic nanobubbles, normalized to the millimolar concentration of Gd-DOTP complex, was calculated according to the following equation (1):

$$r_1 = (R_{1obs} - R_{1dia})/[Gd] \qquad (1)$$

where R_{1dia} is the relaxation rate of a nanobubble suspension without the paramagnetic agent, and [Gd] is the millimolar concentration of the Gd(III) complex in the suspension.

US imaging

The ability of the nanobubbles to generate echogenicity was verified in vitro on a Vevo® 2100 (Visualsonics) ecographer. Nanobubbles were inserted in a capillary embedded in agar gel phantom at constant flow. Echogenic images were visualized using Power color Doppler modality (transducer operating at 32 MHz).

Physico-chemical characterization of nanobubble formulations

Mean hydrodynamic diameter, polydispersity index (PDI), electrophoretic mobility, and zeta potential were determined by photocorrelation spectroscopy (PCS) using a 90 Plus instrument (Brookhaven, NY, USA), red laser = 633 nm at a scattering angle of 90° and at a temperature value of 25 °C, setting refractive index and viscosity values at 1.336 and 1.65 cP respectively. The samples were diluted with filtered water. Each measured value was the average of ten readouts. For zeta potential determination, samples of the nanobubble formulations were placed in the electrophoretic cell, where an electric field of about 14 V/cm was applied. The viscosity of the theranostic nanobubble formulations was determined at 25 °C using a Ubbelohde capillary viscosimeter (Schott Gerate, Germany). The refractive indexes of theranostic nanobubble

formulations were calculated through a polarizing microscope (Spencer Lens Company, Buffalo, New York).

Morphology analysis

Nanobubble morphology was observed by Transmission Electron microscopy (TEM) using a Philips CM10 (Eindhoven, NL) instrument. The diluted nanobubble aqueous suspensions were sprayed on Formwar-coated copper grid and air dried before observation. Moreover, nanobubbles were also observed using an optical microscope Labovert (Leitz) to verify size and shape modification. In particular, bright light microscopy was used to image the bubble size before and after 3 min insonation (frequency 2.5±0.1 MHz) at 37 °C.

Stability of theranostic nanobubbles

The physical stability of the nanobubbles was evaluated by measuring size and morphology over time. Stability was also evaluated following their exposure to US (frequency 2.5±0.1 MHz, average acoustic pressure distribution value 2.4±0.2 MPa, nominal frequency 50 Hz, and nominal power 30 W). The formulations were evaluated before and after US exposure for 30 seconds, 1, 2, 3 and 5 minutes at 37 °C, following 10 minute to rest, by morphology analysis using optical and TEM microscopy to evaluate the integrity of nanobubble structures.

The relaxivity values of theranostic nanobubbles were tested over time for 20 days at room temperature.

Nanobubble stability was also investigated in lyophilized human serum (Seronorm^{TM} Human, Sero AS, Billingstad, Norway). For this purpose 1 ml of nanobubble aqueous suspension was added to 1 ml of the serum and incubated for 3 h at 37 °C.

Encapsulation efficiency of PLP and Gd-DOTP in theranostic nanobubbles

The encapsulation efficiency of PLP was determined on diluted suspension of nanobubbles (until 1:10 with water at pH 2.0). After 15 minutes of sonication in water bath and subsequent centrifugation, the supernatant was analyzed by spectrophotometry.

The loading capacity was determined on freeze-dried nanobubble samples. Briefly a weighted amount of freeze-dried NBs was diluted in 10 ml of HCl solution 0.1 N; after centrifugation, the supernatant was analyzed by spectrophotometry.

The encapsulation of Gd-DOTP complex was determined relaxometrically after acid mineralization of the suspension [33].

In vitro release of PLP

The *in vitro* release kinetics of PLP from the nanobubbles was determined in the presence and in the absence of US by dialysis bag technique at 37 °C. Three mL of nanobubble aqueous suspension were put in a dialysis bag (cellulose dialysis membrane Spectrapore, cut off =12-14 kDa) and used as donor phase against 120 mL of phosphate buffer 0.01 M at pH 7.4 (receiving phase). PLP release was determined up to 24 h, withdrawing 1 ml of the receiving phase at fixed time and replacing with 1 ml of fresh phosphate buffer.

The release was also monitored after US application (frequency 2.5 ± 0.1 MHz, insonation time = 1 min). After insonation of nanobubbles in the dialysis bag, the drug release was followed for 24 h as previously described. All the withdrawn samples were analyzed spectrophotometrically to evaluate the drug concentration.

MR Imaging

The MRI performance of the nanobubbles loaded with Gd-DOTP was assessed *in vitro* on a Bruker Avance 300 spectrometer (7 T) equipped with a microimaging Micro 2.5 probe.

A standard spin-echo T_1 weighted image was acquired with the following parameters: field of view 11.5x11.5 mm, isotropic matrix 128x, slice thickness 1 mm, echo time 3.3 ms, repetition time 250 ms, number of averages 6.

Determination of the hemolytic activity

For hemolytic activity determination, 100 microliters of theranostic nanobubbles were incubated at 37 °C for 90 min with diluted blood (1:4 v/v) obtained by adding freshly prepared PBS at pH = 7.4. After incubation, nanobubbles-containing blood was centrifuged at 1000 rpm for 5 minutes to separate plasma. The amount of hemoglobin released due to hemolysis was determined spectrophotometrically (absorbance readout at 543 nm using a Duo spectrophotometer, Beckman). The hemolytic activity was calculated to reference with a NBs free diluted blood. Complete hemolysis was induced by the addition of ammonium sulphate (20 % w/v).

Optical microscopy was used to evaluate changes on red blood cell morphology after incubation with the theranostic nanobubbles.

Statistical analysis

The results are expressed as mean ± SD. Statistical analyses were performed using unpaired Student's t-test. A value of $p < 0.05$ was considered significant.

Results and discussion

A multi-step preparation method was purposely tuned for co-loading the two companions (drug and imaging agent) into physically stable nanobubbles. The two compounds (PLP and Gd-DOTP) have different physico-chemical properties and may be loaded in different regions of the nanobubble system. In particular, as amphiphilic molecule, PLP is mostly located at the interface with the perfluoropentane core, while the negatively charged Gd-DOTP complex is electrostatically bound to the cationic chitosan on the surface of the nanobubble.

Perfluoropentane, being liquid at room temperature, allows a simplified set-up of the NB preparation (if compared with the use of gases), and, moreover, its water insolubility yields stable bubbles over time avoiding shrinking phenomena. Moreover, the presence of surfactants can decrease the interfacial tension of perfluoropentane and limit the pressure difference between inside and outside of the bubbles, favoring the formulation stability [34]. Indeed, the addition of Epikuron 200® and PLP ethanol solution to perfluoropentane decrease its surface tension from 15.5 mN/m to 10.4 mN/m.

Chitosan is a natural polysaccharide obtained from the partial deacetylation of chitin, comprising copolymers of randomly distributed β-(1-4)-linked D-glucosamine and N-acetyl-D-glucosamine. It was used as component of the shell of nanobubbles in virtue of its good biocompatibility and the polycationic nature that makes it an ideal compound to form stable supramolecular ion pairs with anions [35].

The association of this polycationic polymer with MRI contrast agents was already investigated [36]. Gd complexes can be attached to chitosan, either by chemical or ionic binding. Previously, Gd-DTPA complexes were conjugated to chitosan nanoparticles able to be further loaded with DNA [37] and Gadolinium chloride was ionically trapped in polyelectrolyte complexes containing chitosan and dextran sulphate showing a decreased cytotoxicity in HUVEC cells [38].

Here, the strategy was to use the negatively charged MRI agent Gd-DOTP as imaging probe for the visualization of the delivery of PLP-loaded NBs.

In this work, two different non-toxic co-surfactants (palmitic acid, C16, and tetradecylphosphoric acid, C14) were used to obtain bubbles with sub-micron size. They affected differently the characteristics of nanobubbles as described below.

To demonstrate the binding of Gd-DOTP to the NBs, longitudinal water protons relaxation rate of suspensions containing a fixed concentration of the MRI agent (0.15 mM) and increasing amount of nanobubbles were measured. Upon increasing NB concentration, the relaxation data displayed the typical hyperbolic saturation profile expected in case of the formation of large supramolecular adducts (Fig. 1B). In fact, it is well established that the binding of a Gd(III) complex with slowly tumbling systems enhances the water protons relaxation rates [39]. For instance, a similar

behavior has been reported for the interaction of Gd-DOTP with Human Serum Albumin (HSA) [40]. As far the comparison between the two NB formulations is concerned, the data reported in Fig. 1B suggested that Gd-DOTP bound slightly stronger to palmitic acid-based nanobubbles (C16-NBs).

The TEM image reported in Fig. 2A showed that the Gd-C16-NBs owns a spherical morphology with a well-defined core-shell structure, and a shell thickness of about 60 nm. Similar shapes were observed for all the other NB formulations.

Table 1 reports the comparison between the physico-chemical data (size, polydispersity index, and zeta potential) of Gd-C16-NBs and Gd-C14-NBs compared with the corresponding values measured for the plain system in the presence of the paramagnetic complex. All the formulations showed polydispersity index values ranging from 0.12 to 0.27, with a narrower dispersion observed for C16-containing NBs. Interestingly, C16 formulations showed also a slightly smaller size (around 10 %) than the C14-containing system, regardless of the presence of Gd-DOTP. We speculated that this size difference may be related to the greater anionic electrostatic charge of C14 (due to the phosphate group) than the one of the palmitic acid (due to a carboxylic group partially dissociated); considering that the two cosurfactants are localized at the interface of the perfluoropentane core, the stronger charge of C14 can disturb the interfacial layer of the nanobubbles causing lateral electrostatic repulsions between the phosphate groups and consequently modifying the interfacial packaging.

Unexpectedly, the loading with the Gd(III) complex reduced the mean diameter of ca. 30 %, regardless of the co-surfactant used. Besides to be a further indirect evidence of the interaction between Gd-DOTP and NBs, this result may be interpreted as the formation of a more packaged structure of the polymer shell caused by the electrostatic interaction with the Gd complex. Interestingly, a similar behavior was already reported with DNA-loaded nanobubbles and polyelectrolyte complexation [22].

A further experimental support to the effective binding of Gd-DOTP to the chitosan NBs was gained by measuring zeta-potential. In fact, the presence of the anionic Gd-complex caused a partial charge neutralization of the bubbles, with a reduction of the zeta potential of *ca.* 30 %; Since the Gd-DOTP complex neutralized only some of the positive charges of the NBs, the residual charges accounted for the good stability displayed by the nanobubbles.

Table 1: Physico-chemical characteristics and relaxivity of the nanobubble formulations

FORMULATION	***Average diameter ± SD (nm)***	***PDI***	***ζ-Potential ± SD (mV)***	***r_1 ($s^{-1}mM^{-1}$)***
C14-NBs	*712±12*	*0.27*	*43.3±1.6*	*-------*
Gd-C14-NBs	*510±10*	*0.24*	*32.8±1.7*	*21.5*
C16-NBs	*651±11*	*0.12*	*40.1±0.9*	*-------*
Gd-C16-NBs	*436±14*	*0.15*	*28.8±1.5*	*23.0*
PLP-C16-NBs	*487±35*	*0.15*	*35.1±3.5*	*--------*
Gd-PLP-C16- NBs	*430±15*	*0.21*	*27.1±2.0*	*19.7*

Due to the binding of the Gd-complex to the NBs, the relaxivity of the MRI agent displayed a four-fold increase with respect to the value of the unbound complex (4.70 $s^{-1}mM^{-1}$ at the same experimental conditions) [30]. Such an enhancement is very similar to that one reported for the Gd-DOTP/HSA adduct [40].

The echogenic properties of the two formulations were then investigated *in vitro* at 25 °C and 37 °C at high spatial resolution (30 μm). Nanobubbles were inserted in a transparent silicon tube embedded in an agar gel phantom and allowed to flow using a peristaltic pump (flow 1 ml/min).

Images in power Doppler modality were acquired. Power Doppler Ultrasound (PDUS) is based on measurement of amplitudes of reflected doppler echoes, and it is therefore able to generate a signal correlated to the presence and transit of nanoparticles. The PDUS evaluation was performed with a 32 MHz frequency transducer (performed at 16 MHz during exposure). Fig. 3A reports the PDUS signal detected at 25°C and 37 °C. Both samples produced a good signal, being higher for the C16-based system at both temperatures (A *vs.* C, and B *vs.* D), as visually demonstrated by the power color Doppler representation.

As PDUS is dependent on density and size of the imaged particles, the signal detected reflected the size increase of the NBs associated with the vaporization of the perfluoropentane core, due to ADV phenomenon. ADV is a physical process in which the pressure waves of US induce a phase transition that cause liquid nanodroplets to form gas bubbles [41]. Furthermore, the nanodroplets to nanobubble conversion was also observed by optical microscopy analysis. Figure 4 reports the size increase of the system upon insonation that represents a proof of concept of the system vaporization. The phenomenon was reversible, and the initial bubble size restored after the stimulus.

Based on the enhanced MRI/US imaging performance, smaller size, and improved polydispersity index, chitosan nanobubbles containing palmitic acid were selected for loading PLP.

Table 1 reports the comparison between the main characteristics of PLP- and Gd-DOTP-loaded nanobubbles.

As revealed by TEM analysis (Fig. 2B), the theranostic nanobubbles maintained a spherical morphology with a well-defined core-shell structure, and a shell thickness of about 60 nm.

The loading of PLP in Gd-C16-NBs was of 7% w/w, with an overall encapsulation efficiency of 78%.

In comparison to PLP-free C16-NBs, the presence of the drug caused a significant decrease in the NBs size (25%), exactly as done by the binding Gd-DOTP (33%), thus providing an indirect demonstration of the encapsulation of the drug within the nanobubble structure. A similar reduction in the diameter (34%) was measured when both the companions were loaded to the NBs, likely due to the attainment of the physical limit of the size of this formulation.

As expected, the zeta-potential of PLP-loaded NBs decreased from 40.1 to 35.1 mV due to the partial neutralization of the positive charges of chitosan operated by the phosphate group of PLP. Again, in analogy to the effect on size, the loading of PLP on Gd-DOTP containing NBs had only a slight effect on zeta-potential, which passed from 28.8 to 27.1 mV.

As far the stability of the Gd-loading is concerned, the change in relaxivity over time may be considered a good marker for this property. The relaxivity of Gd-C16-NBs decreased from 23.0 $s^{-1}mM^{-1}$ to 7.9 $s^{-1}mM^{-1}$ over 20 days. Since the binding of the complex is accompanied by a relaxivity enhancement, this observation reflects the loss of association, *i.e.* the release of the Gd complex from the NBs.

To increase the physical stability of the theranostic bubbles, a solution of Pluronic F68 was added to the formulation. Pluronic F68 is an amphiphilic non ionic block copolymer based on ethylene and propylene oxide units widely used in pharmaceuticals. The role of Pluronic F68 in the formulation is to prevent the NBs aggregation by steric stabilization, which is dominated by solvation effect. As the non ionic stabilizer is added in the nanobubble aqueous suspension, it is adsorbed on the nanobubble shell through an anchor segment, while the other well-solvated tail segment extend into the bulk external aqueous medium, avoiding particle agglomeration.

Pluronic F68 provides an additional protection of the NB shell, thus potentially preventing the displacement of Gd-DOTP. The presence of the copolymer did not affect the size of the NBs, but decreased the zeta-potential to about 22 mV. However, such a value should be high enough to avoid NBs aggregation due to the presence of the steric stabilizer on bubble surfaces.

Importantly, the addition of the copolymer significantly improved the stability of the Gd-DOTP loading, and the relaxivity of Gd-C16-Pluronic-NBs did not change over a period of 20 days.

Huang recently proposed polyacrylic acid shelled nanobubbles stabilized with thermosensitive Pluronic F127 and superparamagnetic iron oxide particles (SPIO, acting as T_2-MRI agents) [42]. This system was very stable, maintaining the particle size distribution comparable to the original distribution after 30 days.

Furthermore, the chitosan nanobubble formulations showed a good physical stability after incubation in plasma at 37°C up to 3 h, without displaying morphology or size changes or aggregation phenomena. This behavior can be related to the presence of a perfluoropentane core still liquid. This stabilization could be due to the small size of the nanodroplets and to the presence of a phospholipid monolayer at the system interface. Sheeran demonstrated that lipid-coated droplets were stable against spontaneous vaporization when brought to physiologic temperature and pressure, but they easily converted to bubbles by acoustic pulsing at relatively low mechanical index [43]. The lipid composition and nanostructure can play an important role in bubble stability by providing a mechanical strength and permeation resistance [44]. For therapeutic applications long-term stability of nanobubbles might be exploited for the accumulation of the nanobubbles at the tumor interstitium.

Theranostic nanobubbles, either Pluronic-coated or uncoated, showed no haemolytic activity *in vitro* (Fig. 5). The percentage of haemolysis induced by the NBs formulations was lower than 1 % after 90 minutes at 37°C, thereby confirming a good biocompatibility of the investigated systems.

Fig. 6 reports the in *vitro* kinetic release of PLP from C16-based NBs measured at 37°C. About 2% of the drug is released after 1 h and no initial burst effect was observed showing the good encapsulation stability of PLP within the nanobubble. Under 1 min of US stimulation at 2.5 MHz, PLP was released to a larger extent, especially in the first minutes after the stimulus, reaching about 8 % of drug after 1 h. The enhanced release profile of the drug after insonation was maintained over time up to 24 h. The insonation conditions did not disrupt the nanobubble structure, as proved by the maintenance of a low and controlled release kinetics. Indeed, the physical stability of the theranostic NBs was observed even after 5 minutes of insonation (data not shown). The presence of lipid monolayer might be the key factor allowing the preservation of the system after insonation.

Finally, the ability of Gd-C16-NBs to generate positive MRI contrast was assessed *in vitro*. The T_{1w} images of the phantom reported in Fig. 3B clearly show the presence of a bright contrast only for the samples containing the NBs loaded with the paramagnetic Gd complex. The MRI performance of the paramagnetic NBs is not affected by the presence of PLP or Pluronic F68 in the formulation.

Conclusions

In the present work, novel theranostic chitosan-based nanobubbles, filled by liquid perfluoropentane, and loaded with the drug PLP and the MRI agent Gd-DOTP were prepared. The structural flexibility of the NBs components and the preparation method allowed an efficient co-incorporation of the theranostic companions. The incorporation of PLP did not affect the core-shell structure of NBs.

The overall stability of the NBs was improved by adding Pluronic F68 in the formulation.
The drug showed a slow and prolonged spontaneous drug release *in vitro* that increased upon US stimulation.
These preliminary *in vitro* measurements demonstrated that the NBs are well detectable either in ecography or MRI. Furthermore, the vaporization of the liquid core occurring at physiologic temperature by ADV process caused the enhancement of the US signal.
The investigated system represents a proof of concept for the feasibility of combined MRI/US detectable drug-loaded chitosan NBs in which the MRI agent is electrostatically bound to the NB surface. The obtained results provide useful insights for the design of multi-task theranostic agents.

Acknowledgments

The research was carried out within the project "Innovative Nanosized Theranostic Agents" (code ORTO114HLF) funded by the University of Torino/Compagnia San Paolo. Financial support from Regione Piemonte (Nano-IGT Project) and Turin University research funds (ex-60 %) are gratefully acknowledged.

References

[1] T. Lammers, S. Aime, W.E. Hennink, G. Storm, F. Kiessling, Acc. Chem. Res., 44,10 (2011) 1029–1038

[2] E. Terreno, F. Uggeri, S. Aime, J. Control. Release, 161,2 (2012) 328-337

[3] S. S. Kelkar and T. M. Reineke, Bioconjugate Chem., 22,10 (2011) 1879–1903

[4] D. Shi, Adv. Funct. Mater., 19,21 (2009) 3356–3373

[5] S. M. Janib, A. S. Moses, J. A. MacKay, Adv. Drug Deliv. Rev. 62,11 (2010) 1052–1063

[6] M. S. Muthu and S. Feng, Expert Opin. Drug Deliv., 10,2 (2013) 151-155

[7] S. Sirsi and M. Borden, Bubble Sci. Eng. Technol., 1 (2009) 3-17

[8] E. C. Unger, T. Porter, W. Culp, R. Labell, T. Matsunaga, R. Zutshi, Adv. Drug Deliv. Rev. 56,9 (2004) 1291–1314

[9] K.W. Ferrara, Adv. Drug Deliv. Rev. 60 (2008), 1097-1102

[10] I. Lentacker, B. Geers, J. Demeester, S. C. De Smedt, N.N. Sanders, Mol. Ther. 18,1 (2010) 101-108

[11] A.L. Klibanov, Med. Biol. Eng. Comput. 47 (2009) 875-882

[12] S. Hernot, A. L. Klibanov, Adv. Drug Deliv. Rev. 60,10 (2008), 1153–1166

[13] N. Nomikou, A. P. McHale, Int. J. Hyperthermia 28,4 (2012) 300–310

[14] A. Bisazza, A. Civra, M. Donalisio, D. Lembo, R. Cavalli, Soft Matter 7 (2011) 10590-10593

[15] R. Cavalli, A. Bisazza, D. Lembo, Int. J. Pharm. 456 (2013) 437-445

[16] T. Yin, P. Wang, R. Zheng, Int. J. Nanomed, 7 (2012) 895-904

[17] M. Ao, Z. Wang, H. Ran, D. Guo, J. Yu, A. Li, W. Chen, W. Wu, Y. Zheng, J. Biomed. Mater. Res. Part B Appl. Biomater. 93B,2 (2010) 551-556

[18] D.R. Anderson, M.J. Duryee, R.P. Garvin, M.D. Boska, G.M. Thiele, L.W. Klassen, Magn. Reson. Imaging. 30,1 (2012) 96-103

[19] J.A. Feshitan, F. Vlachos, S.R. Sirsi, E.E. Konofagou, M.A. Borden, Biomat. 33,1 (2012) 247-255

[20] R. Cavalli, A. Bisazza, A. Rolfo, S. Balbis, D. Madonnaripa, I. Caniggia, C. Guoit, Int. J. Pharm. 378 (2009) 215-217

[21] C. Magnetto, M. Prato, A. Khadjavi, G. Giribaldi, I. Fenoglio, J. Jose, G.R. Gulino, F. Cavallo, E. Quaglino, E. Benintende, G. Varetto, A. Troia, R. Cavalli, C. Guiot, RSC Advances. 4 (2014) 38433-38441

[22] R. Cavalli, A. Bisazza, M. Trotta, M. Argenziano, A. Civra, M. Donalisio, D. Lembo, Int. J. Nanomed. 7 (2012), 3309-3318

[23] E.G. Schutt, D.H. Klein, R.M. Mattrey, J.G. Riess, Angew. Chem. Int. Ed. 42 (2003) 3218-3235

[24] H.D. VanLiew and M.E. Burkard, J. Appl. Physiol. 79,4 (1995) 1379-1385

[25] A. Kabalnov, J. Bradley, S. Flaim, D. Klein, T. Pelura, B. Peters, S. Otto, J. Reynolds, E. Schutt, J. Weers, Ultrasound Med. Biol. 24 (1998) 751-760

[26] O.D. Kripfgans, M.L. Fabilli, P.L. Carson, J.B. Fowlkes, J. Acoust. Soc. Am. 116 (2004) 272-281

[27] R.M. Schiffelers, J.M. Metselaar, M.H.A.M Fens, A.P.C.A Janssen, G. Molema, G. Storm, Neoplasia 7,2 (2005) 118–127

[28] E. Kluza, S. Y. Yeo, S. Schmid, D.W.J. van der Schaft, R. W. Boekhoven, R. M. Schiffelers, G. Storm, G. J. Strijkers, K. Nicolay, J. Control. Rel. 151,1 (2011) 10-17

[29] E. Cittadino, M. Ferraretto, E. Torres, A. Maiocchi, B.J. Crielaard, T. Lammers, G. Storm, S. Aime, E. Terreno, Eur. J. Pharm. Sci 45,4 (2012) 436-441

[30] S. Aime, M. Botta, E. Terreno, P.L. Anelli, F. Uggeri, Magn. Res. Med., 30 (1993) 583-591.

[31] A.D. Sherry, J. Ren, J. Huskens, E. Brucher, E. Toth, C.F.C.G. Geraldes, M.M.C.A. Castro, W.P. Cacheris, Inorg. Chem., 35 (1996), pp. 4606–4612

[32] W. F. Osswald, R. E. McDonald, R. P. Niedz, J. P. Shapiro, R. T. Mayer, Anal. Biochem.**,** 204,1 (1992) 40-46

[33] C. Cabella, S.G. Crich, D. Corpillo, A. Barge, C. Ghirelli, E. Bruno, V. Lorusso, F. Uggeri, S. Aime, Contrast Media Mol Imag, 1,1 (2006) 23–29

[34] J.J. Kwan, M.A. Borden, Adv. Colloids Interface Sci. (2012) 183, 82–99.

[35] M. Dash, F. Chiellini, R.M. Ottenbrite, E. Chiellini, Prog. Polym. Sci., 36 (2011) 981–1014

[36] Y. Huang , B. Cao , X. Yang , Q. Zhang , X. Han , Z. Guo, Mag. Reson. Imaging, 31 (2013) 604–609

[37] V. Darras, M. Nelea, F. M. Winnik, M. D. Buschmann, Carbohydr. Polym., 80,4 (2010) 1137–1146

[38] M. Huang, Z. L. Huang, M. Bilgen, C. Berkland, Nanomed. Nanotech. Biol. Med., 4 (2008) 30–40

[39] S. Aime, M. Botta, E. Terreno, Adv Inorg Chem, 57 (2005) 173-237

[40] S. Aime, M. Botta, S. Geninatti Crich, G.B. Giovenzana, R. Pagliarin, M. Piccinini, M. Sisti, E. Terreno, J. Biol. Inorg. Chem., 2 (1997) 470-479.

[41] C. Lin, W.G. Pitt, BioMed Research International 2013 (2013) 1-13

[42] H-Y. Huang, S-H Hu, S-H Hung, C-S Chiang, H liu, T. Chiu, H. Lai, Y. Chen, S-Y Chen, J. Controlled Rel. 172 (2013) 118-127

[43] P.S. Sheeran, S. Luois, P.A. Dayton, T.O. Matsunaga, Langmuir 27,17 (2011) 10412–10420

[44] P.A. Mountford, S.R. Sirsi, M. A. Borden, Langmuir 30 (2014) 6209−6218

Table and figure legends

Table 1: Physico-chemical characteristics and relaxivity of the nanobubble formulations.

Figure 1: A, Molecular structure of Gd-DOTP complex (left) and prednisolone phosphate (right). B, water protons longitudinal relaxation rate of suspensions containing 0.15 mM of Gd-DOTP and increasing number of NBs/mL (0.5 T, 25°C, pH 5.5).

Figure 2: A, TEM image of Gd-C16 chitosan nanobubbles. B, TEM image of theranostic Gd-C16-nanobubbles.

Figure 3: A, Power-color Doppler US images (40 MHz) for C16- (A and B) and C14- (C and D) chitosan nanobubbles. Top row: 25 °C, bottom row: 37 °C. B, T_1-weighted MR image (7 T, 25°C) of the following NB formulations: 1) Gd-C16-Pluronic-NB, 2) Gd-C16-NB, 3) C16-NB, 4) buffer, 5) PLP-C16-NB, 6) Gd-PLP-C16-NB, 7) Gd-PLP-C16-Pluronic-NB.

Figure 4: Optical images of PLP-C16-NBs: A, at room temperature, B, after 3 minutes of insonation (2.5 MHz) at 37 °C, C, after 10 minutes rest at room temperature following insonation (scale bar 1 μm)

Figure 5: Hemolytic activity of theranostic NBs: erythrocytes before (A) and after (B) incubation with theranostic NBs.

Figure 6: *In vitro* release profile of PLP from theranostic NBs at 37 °C in the presence and in the absence of US (1 minute of sonication).

FORMULATION	***Average diameter ± SD (nm)***	***PDI***	***ζ-Potential ± SD (mV)***	***r_1 ($s^{-1}mM^{-1}$)***
C14-NBs	*712±12*	*0.27*	*43.3±1.6*	*-------*
Gd-C14-NBs	*510±10*	*0.24*	*32.8±1.7*	*21.5*
C16-NBs	*651±11*	*0.12*	*40.1±0.9*	*-------*
Gd-C16-NBs	*436±14*	*0.15*	*28.8±1.5*	*23.0*
PLP-C16-NBs	*487±35*	*0.15*	*35.1±3.5*	*--------*
Gd-PLP-C16-NBs	*430±15*	*0.21*	*27.1±2.0*	*19.7*

Table 1: Physico-chemical characteristics and relaxivity of the nanobubble formulations.

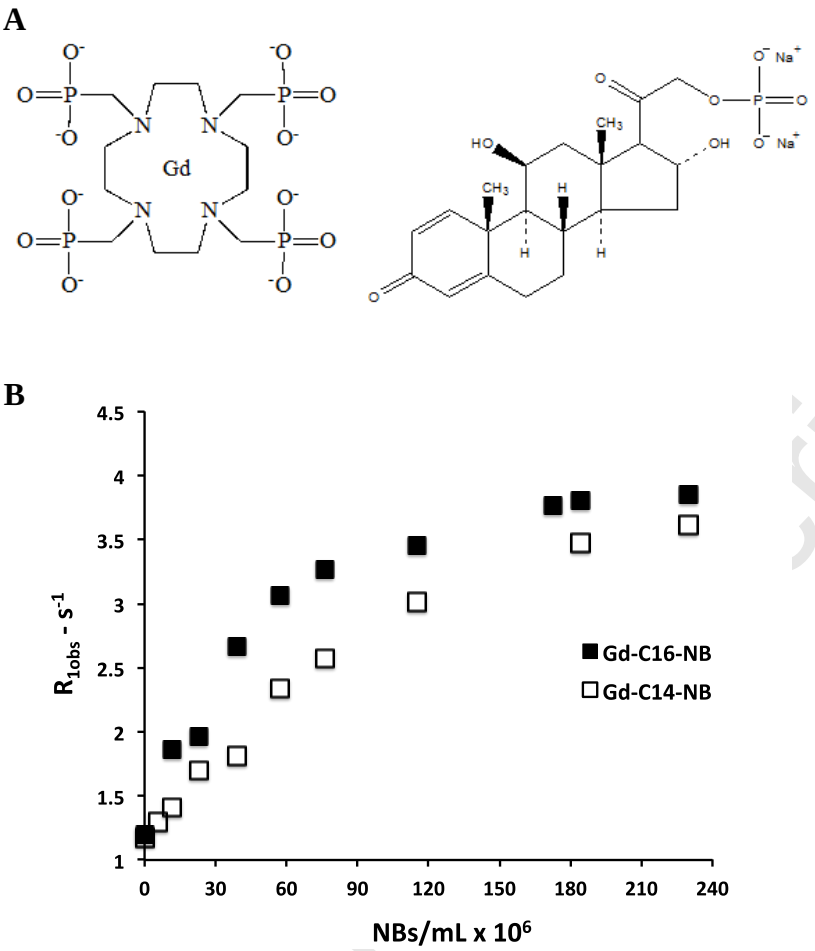

Figure 1: A, Molecular structure of Gd-DOTP complex (left) and prednisolone phosphate (right). B, water protons longitudinal relaxation rate of suspensions containing 0.15 mM of Gd-DOTP and increasing number of NBs/mL (0.5 T, 25°C, pH 5.5).

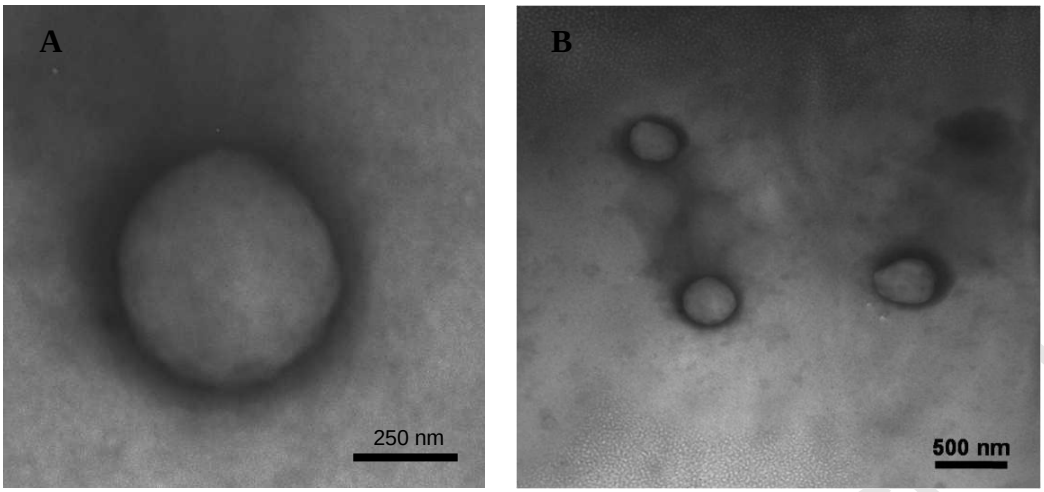

Figure 2: A, TEM image of Gd-C16 chitosan nanobubbles B, TEM image of theranostic Gd-C16-nanobubbles.

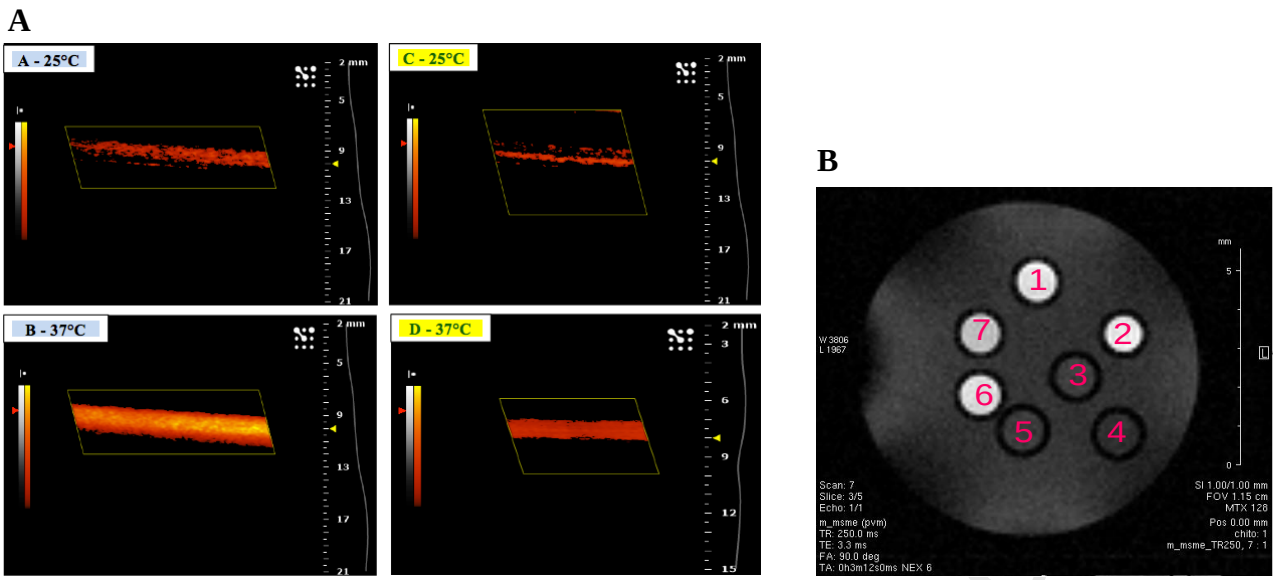

Figure 3: A, Power-color Doppler US images (40 MHz) for C16- (A and B) and C14- (C and D) chitosan nanobubbles. Top row: 25 °C, bottom row: 37 °C. B, T_1-weighted MR image (7 T, 25°C) of the following NB formulations: 1) Gd-C16-Pluronic-NBs, 2) Gd-C16-NBs, 3) C16-NBs, 4) buffer, 5) PLP-C16-NBs, 6) Gd-PLP-C16-NBs, 7) Gd-PLP-C16-Pluronic-NBs.

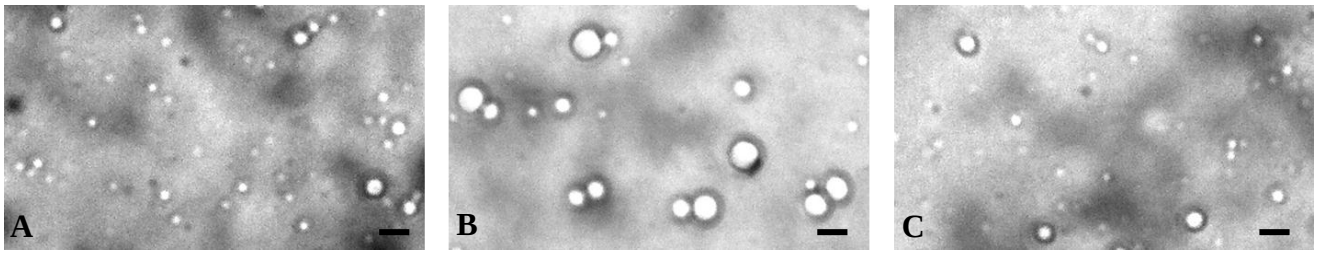

Figure 4: Optical images of PLP-C16-NBs: A, at room temperature, B, after 3 minutes of insonation (2.5 MHz) at 37 °C, C, after 10 minutes rest at room temperature following insonation (scale bars 1 μm)

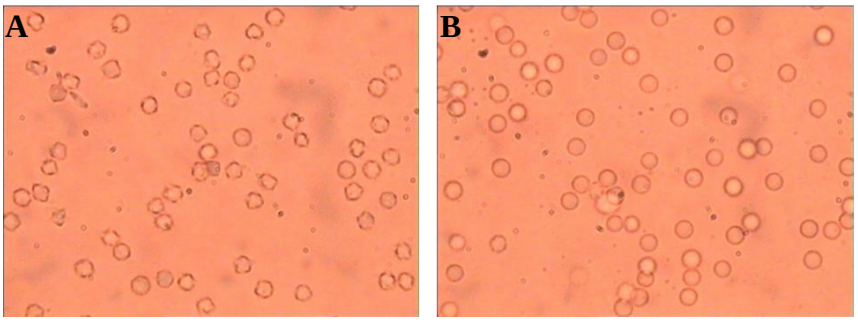

Figure 5: Hemolytic activity of theranostic NBs: erythrocytes before (A) and after (B) incubation with theranostic NBs.

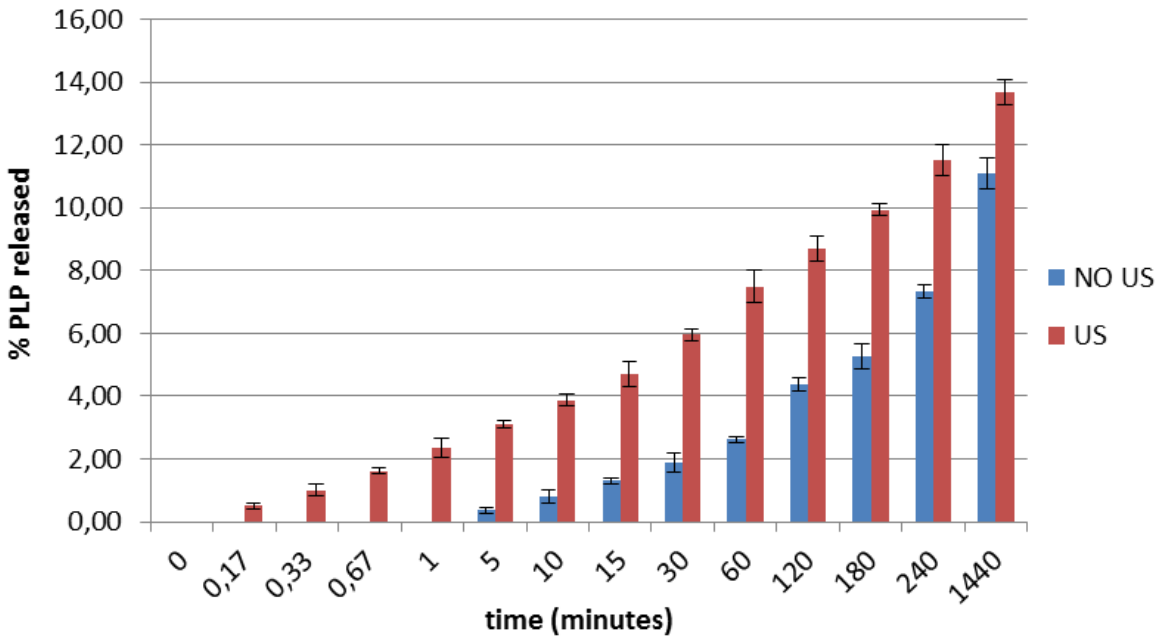

Figure 6: *In vitro* release profile of PLP from theranostic NBs at 37 °C in the presence and in the absence of US (1 minute of sonication).